Author's accepted version. Published in final edited form as: SLAS Technol 2022. doi: 10.1016/j.slast.2022.05.001

This publication has emanated from research supported in part by a grant from Science Foundation Ireland under Grant number SFI/17/CDA/4637. For the purpose of open access, the authors have applied a CC BY public copyright license to any Author Accepted Manuscript version arising from this submission.

A Biomimetic High Throughput Model of Cancer Cell Spheroid Dissemination onto Aligned Fibrillar Collagen

Hossam Ibrahim[1,2], Stephen D. Thorpe[2,3], Michael Paukshto[4], Tatiana S. Zaitseva[4], Wolfgang Moritz[5], and Brian J. Rodriguez[1,2]

[1]School of Physics, University College Dublin, Belfield, Dublin 4, D04 V1W8, Ireland

[2]Conway Institute of Biomolecular & Biomedical Research, University College Dublin, Belfield, Dublin 4, D04 V1W8, Ireland

[3]UCD School of Medicine, University College Dublin, Belfield, Dublin 4, D04 V1W8, Ireland

[4]Fibralign Corporation, 32930 Alvarado-Niles Rd Suite 350, Union City, CA 94587, USA.

[5]InSphero AG, Wagistrasse 27, 8952 Schlieren, Switzerland

Corresponding Author:

Brian J. Rodriguez, School of Physics and Conway Institute of Biomolecular & Biomedical Research, University College Dublin, Belfield, Dublin, D04 V1W8, Ireland.

Email: brian.rodriguez@ucd.ie

Keywords: spheroid culture, collagen, cell migration, image analysis, in vitro models

Abstract

Cell dissemination during tumor development is a characteristic of cancer metastasis. Dissemination from three-dimensional spheroid models on extracellular matrices designed to mimic tissue-specific physiological microenvironments may allow us to better elucidate the mechanism behind cancer metastasis and the response to therapeutic agents. The orientation of fibrillar collagen plays a key role in cellular processes and mediates metastasis through contact-guidance. Understanding how cells migrate on aligned collagen fibrils requires *in vitro* assays with reproducible and standardized orientation of collagen fibrils on the macro-to-nanoscale. Herein, we implement a spheroid-based migration assay, integrated with a fibrillar type I collagen matrix, in a manner compatible with high throughput image acquisition and quantitative analysis. The migration of highly proliferating U2OS osteosarcoma cell spheroids onto an aligned fibrillar type I collagen matrix were quantified. Cell dissemination from the spheroid was polarized with increased invasion in the direction of fibril alignment. The resulting area of cell dissemination had an aspect ratio of 1.2 ± 0.1 and an angle of maximum invasion distance of 5° ± 44° relative to the direction of collagen fibril alignment. The assay described here can be applied to a fully automated imaging and analysis pipeline for the assessment of tumor cell migration with high throughput screening.

Introduction

Cell migration is a critical cell function that dictates the position of cells within the body and plays a key role in embryonic development, wound healing, and metastasis. Cells can migrate by means of a broad repertoire of processes which can be described as single-cell (e.g., amoeboid, mesenchymal) and collective migration (cell sheets, clusters, and streams).[1] Commonly-employed two-dimensional (2D) Boyden chamber and scratch wound assays utilize flat monocultures that do not account for heterogeneity in nutrient and oxygen gradients or cell-cell interactions.[2,3] The former is based on two medium-containing chambers separated by a rigid porous membrane through which cells transmigrate, often in response to a chemokine gradient, with small pores impeding collective migration.[4] This method is not optimal for real-time imaging as cells can become trapped within the porous membrane. The scratch wound assay is typically performed on a rigid 2D tissue culture plate, which can be coated with extracellular matrix (ECM) and involves the migration of cells from dense monolayer sheets to occupy empty regions.[4] Planar 2D monoculture models have been used previously to recapitulate the mechanical basis of wound closure dynamics of epithelial sheets,[5,6] but they tend to fail in describing migration in fibrous tissue.

Cells cultured on patterned and grooved interfaces change their shape, orientation, and direction of movement in response to topographical cues through a phenomenon called contact-guidance. Contact-guidance enables cells to take the path of least resistance when confronted with heterogeneous environments, supporting the notion of preferential migration along ECM interfaces, or aligned structures. Current advances in micro-nanotechnologies and biomaterial engineering offer high-level precision and repeatability in manufacturing structured templates to investigate how biophysical cues can influence tissue morphogenesis. Over the years, researchers have implemented various topographical geometries such as

grooves and ridges.[7,8] Furthermore, adhesive micropatterns,[9] have emerged as a valuable tool to investigate the influence of micro-nano structures on cellular processes and migration. However, in many instances, these templates do not probe the influence of biological or biologically-relevant topographical features present *in vivo*. Instead, studies utilize geometries with edge-like features such as ridges, grooves, pillars, and posts that are not relevant to the *in vivo* environment.[7] In this context, the *in vivo* environment surrounding or associated with the epithelia are edgeless and exhibit fibrillar and curved topographies on the cellular scale.[10] Furthermore, due to the use of synthetic polymer-based materials, these templates exclude ECM remodeling or proteolytic degradation mediated by matrix metalloproteinases to navigate through confined spaces.[11] Therefore, fibrillar and edge-less topographies are needed to investigate cell migration in the context of cell contact-guidance and morphogenesis.

Three-dimensional (3D) models, such as spheroids, have gained considerable attention due to their enhanced physiological relevance to the *in vivo* scenario.[12] As a result of the combined effect of physiological gradients and complex 3D cell-cell interactions,[13,14] spheroids are able to better mimic the *in vivo* environment, making them a useful tool in preclinical drug testing and basic research.[15] Current work in this area focuses on the development of migration assays combining 3D models and ECM components that can facilitate improved reproducibility, increased throughput,[12] and generation of quantitative data.[16]

The architectural features and mechanical properties of the ECM are key regulating factors associated with tumor progression.[17] It has been shown that invasive cancer cell behavior can be controlled by tuning ECM microarchitecture in breast cancer.[18] Thus, it is important to understand cancer cell dissemination as it relates to fibrillar matrix alignment. At the onset of cancer migration, cells released from the tumor encounter heterogeneities in the surrounding tissue matrix, resulting in various degrees of ECM confinement around epithelial tumor

cells.[19,20] Collagen type I, the main component of ECM in interstitial tissues, determines the spatial organization and stability of connective tissues.[21] Cells interacting with these matrices often align with the orientation of collagen fibrils, suggesting that the alignment of the fibrillar architecture can provide structural and signaling cues for cell polarization.[22,23] Several studies have shown that collagen type I has major implications in bone metastases formation from various primary tumors,[24–27] and in the case of osteosarcoma, metastasis from bone to other sites.[28] Fibrillar collagen type I is often heavily deposited in the stroma adjacent to tumors.[29] In addition, it has been reported that a high-density fibrillar collagen matrix is a potent inducer of invadopodia in cancer-associated cells and primary human fibroblasts.[30] In this context, we reason that the aligned fibrillar collagen matrix could also be used to mimic aspects of tumor cell dissemination relevant to the tumor stromal microenvironment.

Most spheroid-migration assays lack high throughput compatibility when it comes to the generation of spheroids *in situ*. Subsequent manual transfer to specialized plates for assessing cell migration adds further complexity and unintended biophysical stimuli to the spheroids. Spheroid-migration assays have been performed before on ECM coated surfaces [3,31,32] or embedded within gels (e.g., Matrigel, collagen).[11,33,34] Spheroid cell invasion matrices usually consist of randomly oriented fibrils and therefore provide little information about cellular interaction with the aligned architecture of collagen fibrils commonly present *in vivo*.[35] Such assays can suffer from low reproducibility of the ECM components and architecture due to polymerization conditions leading to variations in the matrix porosity and fibrillar properties,[36] which may alter the physiochemical response of the cells and the migration process. These matrix variations are a major concern when comparing results in literature due to the diversity of conclusions reported.[37,38] Liquid crystal printing technology provides a method to fabricate reproducible matrices with aligned fibrillar collagen, providing control

over key variables including stiffness, chemistry, and fibrillar architecture without the need for synthetic ECM analogues.[39–41]

Here we aim to develop a biologically relevant migration assay to replicate aspects of tumor cell invasion onto an aligned ECM. We develop a system which facilitates the transfer of homogenous spheroid cultures to the center of a fibrillar type I collagen coated multi-well plate. We use atomic force microscopy (AFM) to resolve the fibrillar matrix topography and stiffness by determining the fibril size and elastic modulus. We demonstrate high throughput capabilities by assessing the suitability of the transfer adapter to mitigate/eliminate the manual handling of spheroid from the hanging drop to the center of the individual well. In addition, we provide basic protocols for imaging and analysis of spheroid dissemination.

Materials and Methods

Aligned Fibrillar Collagen Surface Modification

Purified monomeric atelocollagen solution (porcine type I) at a concentration of 45 mg/mL was prepared by Fibralign Corporation (Union City, CA) to reach a liquid crystal state. Collagen solution was then sheared onto ~0.17 mm thick polycarbonate sheets using a liquid film applicator assembly[42] with a coating speed of 100 mm/s. This resulted in a 2 ± 1 μm thick porcine collagen type I matrix deposited on a 110 mm × 30 mm area of the plastic sheet, sufficient to span three rows of 12 wells (36 wells) when attached to a bottomless 96-well plate (MuWells, San Diego, CA).

Characterization of Surface Topography

AFM was used to characterize the topography and alignment of the fibrillar collagen matrix. The fibrillar collagen matrix was measured in amplitude modulation mode in air using an Asylum Cypher S system (Oxford Instruments) fitted with a Si cantilever probe (Scout 350, Nu Nano). The nominal spring constant and resonant frequency of the cantilever used was 42

N/m and 350 kHz, respectively. The mean fibril diameter was determined from height maps using Asylum Software (Oxford Instruments) as the full-width at half maximum of the height profile transecting randomly chosen fibrils. The orientation of the fibrillar collagen matrix was measured in Fiji using the OrientationJ plugin.[43] The methods used in the OrientationJ plugin to estimate the local orientation of fibrillar collagen structures in an image were extensively discussed by Rezakhaniha et al.[44] The height image (30 μm × 30 μm) was utilized to determine orientations of fibrillar collagen. First the height map was loaded into Gwyddion (open-access scanning probe microscopy (SPM) software) and saved as a tiff image for orientation assessment. The tiff image was loaded into Fiji and the following preprocessing was implemented; image brightness was adjusted to make full use of the available gray value range, and a threshold was applied upon which the image was binarized (Suppl. Fig. S1).

Characterization of Fibrillar Collagen Mechanics

The mechanical properties of the fibrillar collagen layer were also assessed using AFM. The fibrillar collagen matrix was hydrated in phosphate buffered saline (PBS; Sigma-Aldrich, Arklow, Ireland) 2 h prior to mechanical characterization, and force indentations were carried out in PBS. Measurements were conducted in a temperature-regulated room (20–21°C) using an Asylum MFP-3D system (Oxford Instruments) integrated with an Olympus IX71 optical microscope. All-in-one tipless cantilevers (Budget Sensors, Sofia, Bulgaria) with a nominal spring constant (k) of 2.7 N/m were functionalized with a borosilicate sphere of 5 μm radius (Whitehouse Scientific, Waverton, UK) attached to the cantilever end. The cantilever spring constant was obtained experimentally (k = 3.6 N/m) using the Sader method.[45] Force volume mapping mode was used to determine the Young's modulus through application of the Hertz model. A 20 × 20 array of force indentations separated by 2 μm spacing over a 40 μm × 40 μm area (400 indentations per force map) was generated using a calibrated force set-point of

15 nN. To obtain the elastic modulus, the extension part of the force-displacement curves was fit to the Hertz model with an assumed Poisson ratio (ν) of 0.5 [46] using Asylum curve fitting software.

Spheroid Assay Platform Integration

Spheroids were generated using a modified hanging drop technique. The GravityPLUS™ system (InSphero, Schlieren, Switzerland) enables the generation of a hanging drop culture by top loading in a 96-well plate format in a manner amenable to high throughput spheroid generation. U2OS osteosarcoma epithelial cells were cultured in tissue culture flasks (Sigma–Aldrich) until 80% confluence in Dulbecco's Modified Eagle's medium (DMEM, Sigma-Aldrich) supplemented with 10% fetal bovine serum (Gibco, Biosciences, Dun Laoghaire, Ireland), which was exchanged every 3 days. Cells were incubated at 37 °C, with 95% humidity and 5% CO_2 and cultured to passage 26. To generate spheroids, 40 µL of cell suspension containing 500 cells was delivered from the top through the SureDrop™ inlet funnels of the individual GravityPLUS™ plate wells and cultured for 4 days to facilitate spheroid formation. To transfer the hanging drop cultures to the center of fibrillar collagen coated wells in a 96-well plate, an adapter unit was designed, and 3D printed. The adapter unit was printed from rigid acryl resin (AR-M2) with water-soluble acryl resin used as a support material (AR-S1, both Keyence Co., Osaka, Japan) using a high-resolution 3D printer (Agilista-3000, Keyence) with 15 µm print resolution by Hubs B.V. (Amsterdam, The Netherlands). The 3D printed adapter was gently placed into the collagen-coated well plate. Using a multichannel pipette, 70 µL of cell media was dispensed into the SureDrop™ well inlets, which dislodged the hanging spheroid. The adapter ensured that spheroids were guided to the center of the collagen-coated wells. Spheroids were incubated for 45 min until attachment was observed, then the GravityPLUS™ plate and adapter were removed from the collagen-coated plate and each well was topped up with 150 µL of cell culture media.

Microscopy and High Content Imaging

Brightfield images of spheroids at the point of transfer to the collagen-coated plate (t0) were captured using a 10× objective on an inverted brightfield microscope (Olympus CKX53), fitted with a color camera (VC.3031 HD-Lite, Euromex) and Exfocus 0.5× reducing lens (Tucsen). Cell migration from the spheroid body was tracked and imaged using 5× and 10× objectives every 24 h for 96 h using bright-field microscopy (Opera Phenix High Content Screening System, Perkin-Elmer, Beaconsfield, United Kingdom). Spheroid cultures were fixed at 96 h. Cell media was removed, and samples are washed three times with PBS. Fixation was performed by immersing the samples in 4% paraformaldehyde (Sigma-Aldrich) for 30 min followed by cell permeabilization using 0.1% Triton X-100 (Sigma-Aldrich) for 45 min. The samples were washed three times with PBS, incubated with 5% bovine serum albumin (Sigma-Aldrich) in PBS for 30 min, followed by three PBS washes. Cultures were incubated for 2 h at room temperature in Hoechst 33342 (1 µg/mL, Sigma-Aldrich) and Alexa Fluor 568 conjugated phalloidin (300 µg/mL; Invitrogen, Biosciences) in PBS, to label cell nuclei and filamentous (F-)actin, respectively. The samples were then washed three times with PBS before imaging using confocal microscopy at 5× and 10× with 16-bit images obtained (Opera Phenix High Content Screening System).

Spheroid Dissemination and Cell Migration Analysis

Brightfield images of spheroids at the point of transfer to the collagen-coated plate (t_0) were segmented and classified using a FIJI plugin (Trainable Weka segmentation).[47] The F-actin-stained images (t_{96}) were adjusted and analyzed using a custom-made code implemented in MATLAB R2019b (MathWorks, Galway, Ireland) unless otherwise stated. See Supplemental Materials for the code used and a detailed description of the method. The code utilized built-in image processing functions useful for measuring properties of shapes in a binary image such as *bwlabel* and *regionprops*. The image-analysis pipeline was broken into three stages:

(1) preprocess image (acquire, enhance, adjust, filter, threshold); (2) define objects (smooth, denoise, clean, segment); and (3) measure parameters (length, shape descriptors, morphology) (Suppl. Figs. S2 and S3).

Pre-processing methods (Suppl. Fig. S2) were employed to enhance contrast and improve segmentation by utilizing common filtration techniques, followed by histogram-assisted thresholding to outline the periphery of the spheroid and cells. The threshold parameter controlled the cut-off value of the pixel intensity histogram. A mask was applied after applying the threshold and the boundary of the mask was extracted to serve as the contour of the objects before final conversion to a binary image. The spheroids were treated to seven image processing operations on the raw grayscale image. Briefly, (i) increase contrast; (ii) threshold to remove brightest region; (iii) increase brightness of remaining darker cells protruding from the spheroid and apply threshold; (iv) adjust brightness of remaining cells and apply threshold; (v) content that fails to meet the threshold criteria on the third round is removed (leftover content; Suppl. Fig. S2: step 5); (vi) binarize; (vii) remove non-cellular artifacts (outliers) from binary image (after rigorous inspection of F-actin and DNA stained fluorescent images). The obtained binary image was used for measurement of morphology and shape features. The object segmentation method distinguishes between the spheroid bulk invasion, and migrated cells isolated from the spheroid body. Isolated cells were identified as those that are disconnected or dissociated from the continuous disseminated cell sheet (Suppl. Fig. S3).

Objects were analyzed, and the following parameters were extracted using the function *regionprops* for each spheroid: area, centroid, perimeter, orientation, solidity, circularity, and aspect ratio. Additional functions were applied using custom code to extract the following additional parameters at 0 h post transfer to ECM (t_0): spheroid equivalent radius; and at 96 h post transfer to ECM (t_{96}): invasion area, average maximum migration, maximum invasion

distance and angle for the disseminated contiguous spheroid mass, cell migration distance, angle of isolated dissociated cells, disseminated spheroid equivalent radius, spheroid core equivalent radius. See Supplemental Table S1 for definitions of measured parameters. Plots were generated in MATLAB.

Data Analysis

Data presented as mean ± standard deviation unless otherwise specified.

Results

Characterization of Aligned Fibrillar Collagen ECM

To recapitulate the heterogeneity in migration modes, we used a nanoscopically-defined fibrillar collagen matrix to investigate spheroid cell migration with respect to fibril orientation. AFM revealed that the collagen scaffold comprises interconnected, aligned, and crimped collagen fibrils with mean fibril diameter of 298 ± 87 nm (n = 25; Fig. 1A). The aligned fibrillar scaffold did not exhibit the D-band periodicity of ~ 67 nm present in native collagen type I fibrils,[46,48,49] as noted previously in AFM studies of similar films.[50] The local orientation of the fibrillar collagen matrix was assessed and the distribution had a major central peak at -0.5° from the horizontal (Suppl. Fig. S1). Note, calculated fibril orientation will depend on the alignment of the cantilever with the sample with an associated error of ±2°. Additional smaller peaks in fibril orientation were observed at ±90°, -44.5°, and +44.5°. From AFM indentation measurements in PBS, we determined the Young's modulus of the fibrillar collagen ECM to be 26.51 ± 8.41 kPa (n = 400 indentations; Fig. 1B). These values are in agreement with those obtained by Artym et al. using AFM, who report an effective elastic modulus of 56 ± 29 kPa for a cross-linked, hydrated collagen fibrillar matrix.[30]

Spheroid Assay Platform Integration

To address key challenges associated with the use of spheroids as a potential migration model, we developed an assay platform that (1) provides for simplified assay setup through *in situ* spheroid formation and transfer to a fibrillar ECM for assessment of migration, and (2), enables quantitative analysis compatible with high throughput imaging. Figure 2 provides an overview of the developed assay platform. To avoid manual handling of spheroids, a transfer adapter was developed to interface between the hanging drop GravityPLUS^{TM} plate and the underlying ECM coated plate. The transfer adapter ensured that each spheroid is positioned in the center of the well without damaging the underlying fibrillar collagen matrix. Central positioning of the spheroid is important to ensure that cell dissemination can occur in all directions from the spheroid mass, in addition to simplifying subsequent high throughput imaging procedures.

U2OS osteosarcoma cells were used to generate spheroids. Upon seeding of 500 cells per well in the GravityPLUS^{TM} plate, hanging drops formed at the well outlets and the cells aggregated to form microtissues by gravity-enforced assembly over 4 days (Fig. 2E). Spheroids were transferred using the transfer adapter to the fibrillar collagen coated base plate. Upon spheroid contact, cells attached and migrated along the 3D topographical cues provided by the aligned collagen.

High Throughput Spheroid Outgrowth Analysis

The extent, direction, and persistence of cell dissemination from a spheroid are factors of both the spheroid properties (e.g., cell phenotype and nutrient gradients) and the fibrillar ECM (e.g., contact guidance). Herein, we describe methods to quantitively assess the shape, growth area, distance, and orientation of spheroid dissemination onto an ECM substrate. To capture the diversity in spheroid dissemination, all spheroids were seeded onto aligned fibrillar collagen and cultured for 96 h to facilitate cell migration and outgrowth from the

spheroid mass. 12 representative spheroids are shown in Figure 3A. All spheroids are positioned in the central field of each well (Suppl. Fig. S4). To better visualize the pattern and extent of cell migration from the spheroid mass, cells are fluorescently stained for DNA and F-actin. F-actin provides an approximation of the cell's projected area and the fluorescent signal is used to quantify cell outgrowth from the spheroid (Fig. 3C, E). Figures 3F-I depict the binary output obtained using our custom image analysis methods with total projected outgrowth (Fig. 3F), contiguous spheroid outgrowth (Fig. 3G), the spheroid core (Fig. 3H), and cells that have dissociated from the contiguous spheroid mass through migration (Fig. 3I). The influence of aligned fibrillar collagen scaffold on U2OS spheroid morphology and outgrowth was determined by analyzing the processed binary images (Fig. 3F-I). The extent of spheroid dissemination is assessed using objective shape characteristics including circularity, solidity, the aspect ratio of the best fit ellipse and its orientation. To characterize the extent of contiguous dissemination from the spheroid, the shape of the boundary and radial distance from the centroid to each pixel x(n), y(n) on the boundary were assessed (Fig. 3J). In addition, cellular dissociation events, defined as a cell or group of cells splitting away from the disseminating cell sheet, were quantified and categorized into three classes, single cells (1 cell), doublet (2 cells), and clusters (> 2 cells) following the example of Lam et al.[51] to elucidate the extent of heterogeneity in migration.

Upon attachment to fibrillar matrix, the cells dissociate and spread outwards from the spheroid mass. The extent of spheroid dissemination and migration onto the fibrillar ECM was determined, considering both the contiguous cell sheet and dissociated single cells due to the biological significance of leader cells,[52] which may indicate metastatic potential.[53] Briefly, to calculate average maximum migrating distance, the equivalent radius was calculated based on the projected area of the spheroid core at 0 h as it was transferred to the ECM, represented by the red circle (Fig. 4A). A convex polygon represents the perimeter of

the migrating cell front including single cells. The average maximum migrating distance at 96 h was calculated as the *(Perimeter of the polygon/2π) – Radius of core circle*)[54]. It is important to note that the *Avg. of max migrating distance* is more applicable when the cells move collectively with few cells migrating far away.[33] To assess collective cell sheet invasion, the projected area of the enlarged spheroid core (orange region, Fig. 4A) was subtracted from the area of contiguous cells (blue region, Fig. 4A) and was observed to be 0.3191 ± 0.1049 mm^2. The angle of maximum invasive protrusion distance (α_s) from the centroid (Fig. 4A) was also determined from the contiguous spheroid binary image at 96 h and produced an average invasion angle of $5 \pm 44°$. See Supplemental Figure S5 for box plots for contiguous spheroid measurements.

In addition to assessing separate regions of the disseminated spheroid, we also describe the contiguous cell sheet dissemination. In Figure 4B we perform the measurement on the contiguous filled spheroid binary image which excludes disconnected migrating cells (see Suppl. Fig S3 part 9). Using dimensionless shape descriptors, the average circularity ratio of 0.08 ± 0.02 was determined for spheroids on aligned fibrillar collagen and infers that the shape of spheroid dissemination departs significantly from a circular geometry (with 1 corresponding to a perfect circle). The aspect ratio (AR) was measured by considering the major/minor axes of the fitted ellipse (Fig. 4B) and describes the elongation of the spheroid. It was larger than 1 with an average value of 1.2 ± 0.1 (Suppl. Fig. S5E), denoting spheroids with polarized dissemination morphologies, consistent with the circularity results. To determine the overall orientation of the spheroid in degrees ranging from -90 to 90° relative to the macroscopic collagen fiber alignment, the angle (θ) between the major axis of the ellipse rotated clockwise from the x-axis was measured, resulting in an average orientation angle (θ_S) of $-4 \pm 39°$ (Fig. 4B, Suppl. Fig. S5D). Additionally, an average solidity ratio of

0.75 ± 0.05 was determined from the contiguous filled spheroid and is a measure of boundary irregularity; a more irregular boundary has a lower solidity ratio.[55]

When observing U2OS spheroid migration on aligned fibrillar collagen, a diversity of migration modes was evident. The perimeter of the contiguous cell sheet (excluding disconnected cells) displayed an irregular shape at 96 h (Fig. 3J, Suppl. Fig. S6: raw signature analysis), with cellular protrusions extending out from the spheroid mass via collective migration in the shape of finger-like collective strands on the aligned fibrillar matrix (Fig. 5). In addition, the single migrating cells exhibit lamellipodia and filopodia demonstrating interactions with the fibrillar collagen ECM (white arrows, Fig. 5B).

Cellular dissociation from the contiguous spheroid-associated cell sheet can also be quantified. This analysis is illustrated in a representative spheroid in Figure 6 where a total of 37 dissociation events were detected, with 41% as single cells (n = 15), 14% as doublets (n = 5), and 46% as clusters (n = 17; Fig. 6 A-E). Analysis of U2OS cell dissociation from the cell sheet across 34 spheroids revealed that 48% of the events were single-cells, whereas 19% and 33% were doublets and clusters, respectively (Suppl. Figs. S7 and S8). These results show that the assay allows diverse migration modes, and the migration mode is almost 50% single and 50% multi-cellular. In that respect, the assay might be suitable for a variety of migration assessments and can be applied to investigate various cellular locomotive concepts including endothelial to mesenchymal transition, collective migration, and colony formation.

The fibrillar topography was sufficient to polarize the spheroid sheet migration and elicit fibroblastic and mesenchymal-like elongated migration phenotypes (Figs. 3-5). This was evident from the aspect ratio and orientation data (Table 1), where the aspect ratio recorded for dissociated U2OS cell migration exhibited a mean of 1.7 ± 0.5, with mean orientation of 2 ± 48° with respect to the mean fiber orientation.

Discussion

The spheroid-based migration assay described herein combines spheroids generated by hanging drop culture and an aligned fibrillar collagen ECM to satisfy the requirements for high throughput assay development. It provides for scale, speed, simplicity, reproducibility, and automation in terms of set up, readout, and analysis.

The assay does not damage the underlying matrix or the cells at the migration front as is the case for a wound healing assay. This is facilitated by the integration of a 3D printed transfer adapter positioning the spheroid in the center of the well. The control of the lateral positioning and distribution of the spheroids inside the well leads to further advantages, namely, elimination of spheroid floating in media and adherence to side wall, reduction in time searching for and imaging the spheroid, which subsequently reduces the number of field of views to be imaged to capture spheroid dissemination. Standard staining procedures were applied to visualize the cytoskeleton, which is another advantage compared to embedded systems where post processing is difficult. The results established via our image processing protocol describing spheroid dissemination showed small standard deviations in characterizing the dissemination, thus facilitating quantitative analysis.

The spheroids exhibit a broadly polarized morphology with a mean spheroid orientation (θ_S) - 4 ± 39° and aspect ratio (AR) of 1.2 ± 0.1, albeit to a lesser extent than the dissociated cells (single, doublets, clusters) with a mean orientation (θ_C) of 2 ± 48° and aspect ratio of 1.7 ± 0.5. (Table 1). However, in confirmation of a previous report conducted on fibrillar and aligned collagen-coated substrates with similar properties,[56] we observe that epithelial cell based spheroids such as the U2OS cell line used here do not strongly align along the direction of the collagen fibrils used in this study. Furthermore, morphometric analysis in that report revealed that there were larger number of elongated cells on nanofibrillar collagen than on flat controls, with the 30 nm fibril diameter having more elongated cells than the 300 nm

fibril diameter substrates.[56] Therefore, enhanced alignment might be achieved with U2OS cells on matrices with, e.g., 30 nm fibrils, or with a different cell line on the larger fibril diameter films used in the present study.

The classification of the dissociated events (single, doublet, cluster) was facilitated and made possible by the ability to implement immunofluorescence staining of the actin cytoskeleton and the nucleus DNA to closely verify those migration patterns, while the imaging results showed that fine details can also be extracted in a high throughput manner (Figs. 5, 6). As shown in Figure 5, dissociated events can be extracted, and a range of measurements can be applied to deduce variations between dissociated events across a population of spheroids (Suppl. Fig. S6). An advantage of the migration assay is realized through the permittance of diverse migration modes, with approx. 50% single and 50% multi-cell. In that respect, the assay can be applied to investigate various migration strategies such as endothelial to mesenchymal transition, collective migration, and colony formation. The migration assay strategy could be adapted for use with a range of ECM substrates such as synthetic poly ∈-caprolactone nanofiber scaffolds. Additionally, the assay can be modified to include membrane extracts such as Matrigel to encapsulate the spheroid with a tunable thickness forming a shell to further recapitulate the fundamental complexities of the metastatic process *in vivo*.[57] Cells could be fluorescently tagged with eGFP, cell tracker, or similar labels to facilitate dynamic time lapse assessment of cell dissemination. Altogether, the platform with such modifications would provide a complete toolkit to bridge the gap between 2D assays and the *in vivo* environment.

Conclusions

To accelerate diagnosis and discovery of new therapeutics affecting cell motility and cancer metastasis, cell-based assays should provide tissue-mimicking ECM, allow real-time

visualization, permit phenotypic analysis of cells, and facilitate high throughput screening in standard multi-well plate formats. In this work, a fibrillar collagen type I ECM having a tailored topography and stiffness was used to study contact guidance, tumor spheroid dissemination, and cell migration in a high throughput manner using a 96-well plate format. We validated the 3D printed adapter design to transfer and position spheroids prepared using the hanging drop method to the center of each well. Complementary assessments examined the influence of the aligned ECM on migration descriptors such as shape and area, providing quantitative information related to different migration patterns displayed by a spheroid forming cell line. This migration assay might accelerate diagnosis and help develop new therapeutics by understanding how ECM composition and topography can influence disease progression and cancer metastasis.

Acknowledgments

This research was funded by the European Union's Horizon 2020 research and innovation program under Marie Skłodowska-Curie grant agreement number 644175 and the UCD School of Physics (SIRAT − Scholarship in Research and Teaching). BJR also acknowledges the financial support of Science Foundation Ireland (SFI/17/CDA/4637) and the Sustainable Energy Authority of Ireland (SEAI). We are grateful to Dr. Alex Groisman, Dr. Edgar Gutierrez, and Dr. Eugene Tkachenko (MuWells) for the fabrication of custom-made plates with aligned collagen coating. We thank Dr. Jeremy Simpson for providing the U2OS osteosarcoma cell line. Spheroid imaging was performed via the UCD Conway Imaging Core in the Cell Screening Laboratory of the UCD School of Biology and Environmental Science.

References

1. Friedl P. Prespecification and plasticity: Shifting mechanisms of cell migration. *Current Opinion in Cell Biology*. 2004;16(1):14-23. doi:10.1016/j.ceb.2003.11.001
2. Guy JB, Espenel S, Vallard A, et al. Evaluation of the cell invasion and migration process: A comparison of the video microscope-based scratch wound assay and the Boyden chamber assay. *Journal of Visualized Experiments*. 2017;2017(129):1-7. doi:10.3791/56337
3. Zimmermann M, Box C, Eccles SA. Two-Dimensional vs. Three-Dimensional In Vitro Tumor Migration and Invasion Assays. In: Target Identification and Validation in Drug Discovery, Springer; 2013:227-252. doi:10.1007/978-1-62703-311-4_15
4. Kramer N, Walzl A, Unger C, et al. In vitro cell migration and invasion assays. *Mutation Research - Reviews in Mutation Research*. 2013;752(1):10-24. doi:10.1016/j.mrrev.2012.08.001
5. Anon E, Serra-Picamal X, Hersen P, et al. Cell crawling mediates collective cell migration to close undamaged epithelial gaps. *Proceedings of the National Academy of Sciences of the United States of America*. 2012;109(27):10891-10896. doi:10.1073/pnas.1117814109
6. Sakar MS, Eyckmans J, Pieters R, Eberli D, Nelson BJ, Chen CS. Cellular forces and matrix assembly coordinate fibrous tissue repair. *Nature Communications*. 2016;7(March):1-8. doi:10.1038/ncomms11036
7. Teixeira AI, Abrams GA, Bertics PJ, Murphy CJ, Nealey PF. Epithelial contact guidance on well-defined micro- and nanostructured substrates. *Journal of Cell Science*. 2003;116(10):1881-1892. doi:10.1242/jcs.00383

8. Kilinc D, Blasiak A, Baghban MA, et al. Charge and topography patterned lithium niobate provides physical cues to fluidically isolated cortical axons. *Applied Physics Letters*. 2017;110(5). doi:10.1063/1.4975304

9. Albert PJ, Schwarz US. Modeling cell shape and dynamics on micropatterns. *Cell Adhesion and Migration*. 2016;10(5):516-528. doi:10.1080/19336918.2016.1148864

10. Rougerie P, Pieuchot L, dos Santos RS, et al. Topographical curvature is sufficient to control epithelium elongation. *Scientific Reports*. 2020;10(1):1-14. doi:10.1038/s41598-020-70907-0

11. Wolf K, Wu YI, Liu Y, et al. Multi-step pericellular proteolysis controls the transition from individual to collective cancer cell invasion. *Nature Cell Biology*. 2007;9(8):893-904. doi:10.1038/ncb1616

12. Breslin S, O'Driscoll L. Three-dimensional cell culture: The missing link in drug discovery. *Drug Discovery Today*. 2013;18(5-6):240-249. doi:10.1016/j.drudis.2012.10.003

13. Mehta G, Hsiao AY, Ingram M, Luker GD, Takayama S. Opportunities and challenges for use of tumor spheroids as models to test drug delivery and efficacy. *Journal of Controlled Release*. 2012;164(2):192-204. doi:10.1016/j.jconrel.2012.04.045

14. Hirschhaeuser F, Menne H, Dittfeld C, West J, Mueller-Klieser W, Kunz-Schughart LA. Multicellular tumor spheroids: An underestimated tool is catching up again. *Journal of Biotechnology*. 2010;148(1):3-15. doi:10.1016/j.jbiotec.2010.01.012

15. Fennema E, Rivron N, Rouwkema J, van Blitterswijk C, de Boer J. Spheroid culture as a tool for creating 3D complex tissues. *Trends in Biotechnology*. 2013;31(2):108-115. doi:10.1016/j.tibtech.2012.12.003

16. Driscoll MK, Danuser G. Quantifying Modes of 3D Cell Migration. *Trends in Cell Biology*. 2015;25(12):749-759. doi:10.1016/j.tcb.2015.09.010

17. MacCurtain BM, Quirke NP, Thorpe SD, Gallagher TK. Pancreatic Ductal Adenocarcinoma: Relating Biomechanics and Prognosis. *Journal of Clinical Medicine*. 2021;10(12):2711. doi:10.3390/jcm10122711

18. Carey SP, Kraning-Rush CM, Williams RM, King and CAR. Biophysical control of invasive tumor cell behavior by extracellular matrix microarchitecture. *Biomaterials*. 2012;33(16):4157-4165. doi:10.1016/j.biomaterials.2012.02.029

19. Nasrollahi S, Pathak A. Topographic confinement of epithelial clusters induces epithelial-to-mesenchymal transition in compliant matrices. *Scientific Reports*. 2016;6(January):1-12. doi:10.1038/srep18831

20. Spaderna S, Schmalhofer O, Hlubek F, et al. A Transient, EMT-Linked Loss of Basement Membranes Indicates Metastasis and Poor Survival in Colorectal Cancer. *Gastroenterology*. 2006;131(3):830-840. doi:10.1053/j.gastro.2006.06.016

21. Haeger A, Krause M, Wolf K, Friedl P. Cell jamming: Collective invasion of mesenchymal tumor cells imposed by tissue confinement. *Biochimica et Biophysica Acta* -. 2014;1840(8):2386-2395. doi:10.1016/j.bbagen.2014.03.020

22. Friedrichs J, Taubenberger A, Franz CM, Muller DJ. Cellular remodelling of individual collagen fibrils visualized by time-lapse AFM. *Journal of molecular biology*. 2007;372(3):594-607. doi:10.1016/j.jmb.2007.06.078

23. Hadamitzky C, Zaitseva TS, Bazalova-Carter M, et al. Aligned nanofibrillar collagen scaffolds - Guiding lymphangiogenesis for treatment of acquired lymphedema. *Biomaterials*. 2016;102:259-267. doi:10.1016/j.biomaterials.2016.05.040

24. Zhao H, Han KL, Wang ZY, et al. Value of C-telopeptide-cross-linked type I collagen, osteocalcin, bone-specific alkaline phosphatase and procollagen type I N-terminal propeptide in the diagnosis and prognosis of bone metastasis in patients with malignant tumors. *Medical Science Monitor*. 2011;17(11):626-633. doi:10.12659/msm.882047

25. Cloos PAC, Fledelius C, Christgau S, et al. Investigation of bone disease using isomerized and racemized fragments of type I collagen. *Calcified Tissue International*. 2003;72(1):8-17. doi:10.1007/s00223-002-2034-1

26. Hall CL, Dai JL, Van Golen KL, Keller ET, Long MW. Type I collagen receptor (α2β1) signaling promotes the growth of human prostate cancer cells within the bone. *Cancer Research*. 2006;66(17):8648-8654. doi:10.1158/0008-5472.CAN-06-1544

27. Ferreira AR, Alho I, Shan N, et al. N-Telopeptide of Type I Collagen Long-Term Dynamics in Breast Cancer Patients with Bone Metastases: Clinical Outcomes and Influence of Extraskeletal Metastases. *The Oncologist*. 2016;21(12):1418-1426. doi:10.1634/theoncologist.2015-0527

28. Wei D, Li C, Ye J, Xiang F, Liu J. Extracellular Collagen Mediates Osteosarcoma Progression Through an Integrin α2β1/JAK/STAT3 Signaling Pathway . *Cancer Management and Research*. 2020;12:12067-12075. doi:10.2147/CMAR.S273466

29. Nissen NI, Karsdal M, Willumsen N. Collagens and Cancer associated fibroblasts in the reactive stroma and its relation to Cancer biology. *Journal of Experimental and Clinical Cancer Research*. 2019;38(1):1-12. doi:10.1186/s13046-019-1110-6

30. Artym V., Swatkoski S, Matsumoto K, et al. Dense fibrillar collagen is a potent inducer of invadopodia via a specific signaling network. *Journal of Cell Biology*. 2015;208(3):331-350. doi:10.1083/jcb.201405099

31. Deryugina EI, Bourdon MA. Tenascin mediates human glioma cell migration and modulates cell migration on fibronectin. *Journal of Cell Science*. 1996;109(3):643-652.

32. Lakka SS, Gondi CS, Yanamandra N, et al. Inhibition of cathepsin B and MMP-9 gene expression in glioblastoma cell line via RNA interference reduces tumor cell invasion,

tumor growth and angiogenesis. *Oncogene*. 2004;23(27):4681-4689. doi:10.1038/sj.onc.1207616

33. Liu H, Lu T, Kremers GJ, Seynhaeve ALB, Ten Hagen TLM. A microcarrier-based spheroid 3D invasion assay to monitor dynamic cell movement in extracellular matrix. *Biological Procedures Online*. 2020;22(1):1-12. doi:10.1186/s12575-019-0114-0

34. Ilina O, Bakker GJ, Vasaturo A, Hofmann RM, Friedl P. Two-photon laser-generated microtracks in 3D collagen lattices: Principles of MMP-dependent and -independent collective cancer cell invasion. *Physical Biology*. 2011;8(1). doi:10.1088/1478-3975/8/1/015010

35. Zunder SM, Gelderblom H, Tollenaar RA, Mesker WE. The significance of stromal collagen organization in cancer tissue: An in-depth discussion of literature. *Critical Reviews in Oncology/Hematology*. 2020;151:102907. doi:10.1016/j.critrevonc.2020.102907

36. Roeder BA, Kokini K, Sturgis JE, Robinson JP, Voytik-Harbin SL. Tensile Mechanical Properties of Three-Dimensional Type I Collagen Extracellular Matrices with Varied Microstructure. *Journal of Biomechanical Engineering*. 2002;124(2):214-222. doi:10.1115/1.1449904

37. Wolf K, Mazo I, Leung H, et al. Compensation mechanism in tumor cell migration: Mesenchymal-amoeboid transition after blocking of pericellular proteolysis. *Journal of Cell Biology*. 2003;160(2):267-277. doi:10.1083/jcb.200209006

38. Sabeh F, Ota I, Holmbeck K, et al. Tumor cell traffic through the extracellular matrix is controlled by the membrane-anchored collagenase MT1-MMP. *Journal of Cell Biology*. 2004;167(4):769-781. doi:10.1083/jcb.200408028

39. Paukshto M, Fuller G, Michailov A, Remizov S. Optics of sheared liquid-crystal polarizer based on aqueous dispersion of dichroic-dye nano-aggregates. *Journal of the Society for Information Display*. 2005;13(9):765. doi:10.1889/1.2080515

40. Giraud-Guille MM, Mosser G, Belamie E. Liquid crystallinity in collagen systems in vitro and in vivo. *Current Opinion in Colloid & Interface Science*. 2008;13(4):303-313. doi:10.1016/j.cocis.2008.03.002

41. Besseau L, Coulomb B, Lebreton-Decoster C, Giraud-Guille MM. Production of ordered collagen matrices for three-dimensional cell culture. *Biomaterials*. 2002;23(1):27-36. doi:10.1016/S0142-9612(01)00075-8

42. McMurtry DH, Paukshto M v., Bobrov YA. Liquid film applicator assembly and rectilinear shearing system incorporating the same. Published online October 4, 2011.

43. Schindelin J, Arganda-Carreras I, Frise E, et al. Fiji: an open-source platform for biological-image analysis. *Nature Methods*. 2012;9(7):676-682. doi:10.1038/nmeth.2019

44. Rezakhaniha R, Agianniotis A, Schrauwen JTC, et al. Experimental investigation of collagen waviness and orientation in the arterial adventitia using confocal laser scanning microscopy. *Biomechanics and Modeling in Mechanobiology*. 2012;11(3-4):461-473. doi:10.1007/s10237-011-0325-z

45. Sader JE, Chon JWM, Mulvaney P. Calibration of rectangular atomic force microscope cantilevers. *Review of Scientific Instruments*. 1999;70(10):3967-3969. doi:10.1063/1.1150021

46. Grant CA, Phillips MA, Thomson NH. Dynamic mechanical analysis of collagen fibrils at the nanoscale. *Journal of the Mechanical Behavior of Biomedical Materials*. 2012;5(1):165-170. doi:10.1016/j.jmbbm.2011.08.020

47. Arganda-Carreras I, Kaynig V, Rueden C, et al. Trainable Weka Segmentation: a machine learning tool for microscopy pixel classification. *Bioinformatics*. 2017;33(15):2424-2426. doi:10.1093/bioinformatics/btx180

48. Baldwin SJ, Quigley AS, Clegg C, Kreplak L. Nanomechanical mapping of hydrated rat tail tendon collagen I fibrils. *Biophysical Journal*. 2014;107(8):1794-1801. doi:10.1016/j.bpj.2014.09.003

49. Wenger MPE, Bozec L, Horton MA, Mesquida P. Mechanical properties of collagen fibrils. *Biophysical journal*. 2007;93(4):1255-1263. doi:10.1529/biophysj.106.103192

50. Denning, Denise; Paukshto, M. V.; Habelitz, S.; Rodriguez BJ. Piezoelectric properties of aligned collagen membranes. *Journal of Biomedical Materials Research Part B: Applied Biomaterials, 102 (2): 284-292*. Published online 2014. doi:10.1002/jbm.b.33006

51. Lam H. 3D co-culture spheroid drug screening platform for pancreatic cancer invasion. *Doctoral dissertation, King's College London*. Published online 2018.

52. Riahi R, Sun J, Wang S, Long M, Zhang DD, Wong PK. Notch1-Dll4 signalling and mechanical force regulate leader cell formation during collective cell migration. *Nature Communications*. 2015;6:1-11. doi:10.1038/ncomms7556

53. Scarpa E, Mayor R. Collective cell migration in development. *Journal of Cell Biology*. 2016;212(2):143-155. doi:10.1083/jcb.201508047

54. Merkus HG. *Particle Size Measurements: Fundamentals, Practice, Quality*. Vol 17. Springer Science & Business Media; 2009.

55. Pasqualato A, Lei V, Cucina A, et al. Shape in migration: Quantitative image analysis of migrating chemoresistant HCT-8 colon cancer cells. *Cell Adhesion and Migration*. 2013;7(5):450-459. doi:10.4161/cam.26765

56. Muthusubramaniam L, Peng L, Zaitseva T, Paukshto M, Martin GR, Desai TA. Collagen fibril diameter and alignment promote the quiescent keratocyte phenotype. *Journal of Biomedical Materials Research - Part A*. 2012;100 A(3):613-621. doi:10.1002/jbm.a.33284

57. Guzman A, Sánchez Alemany V, Nguyen Y, Zhang CR, Kaufman LJ. A novel 3D in vitro metastasis model elucidates differential invasive strategies during and after breaching basement membrane. *Biomaterials*. 2017;115:19-29. doi:10.1016/j.biomaterials.2016.11.014

Tables and Table Legends

Table 1. Shape descriptors for spheroid dissemination and dissociated events. Mean ± standard deviation, $n_{spheroid} = 34$, $n_{dissociated\ event} = 1{,}384$.

Property	**Spheroid**	**Dissociated events**	**Circle**
Aspect ratio (AR)	1.2 ± 0.1	1.7 ± 0.5	1
Circularity	0.08 ± 0.02	0.69 ± 0.30	1
Orientation (θ_s, θ_c)	-4 ± 39°	2 ± 48°	-
Solidity	0.75 ± 0.03	0.83 ± 0.13	1

Figures and Figure Legends

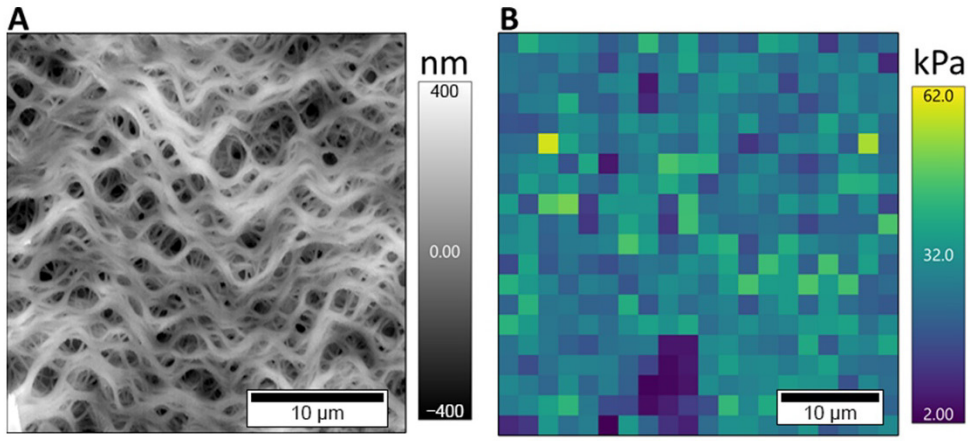

Figure 1. Topography and Young's modulus of the aligned fibrillar collagen matrix. A: Representative AFM height image of fibrillar collagen topography (30 µm × 30 µm scan size). B: Representative force-volume map (40 µm × 40 µm area) conducted on fibrillar collagen matrix hydrated in PBS. Color represents Young's modulus from each force curve.

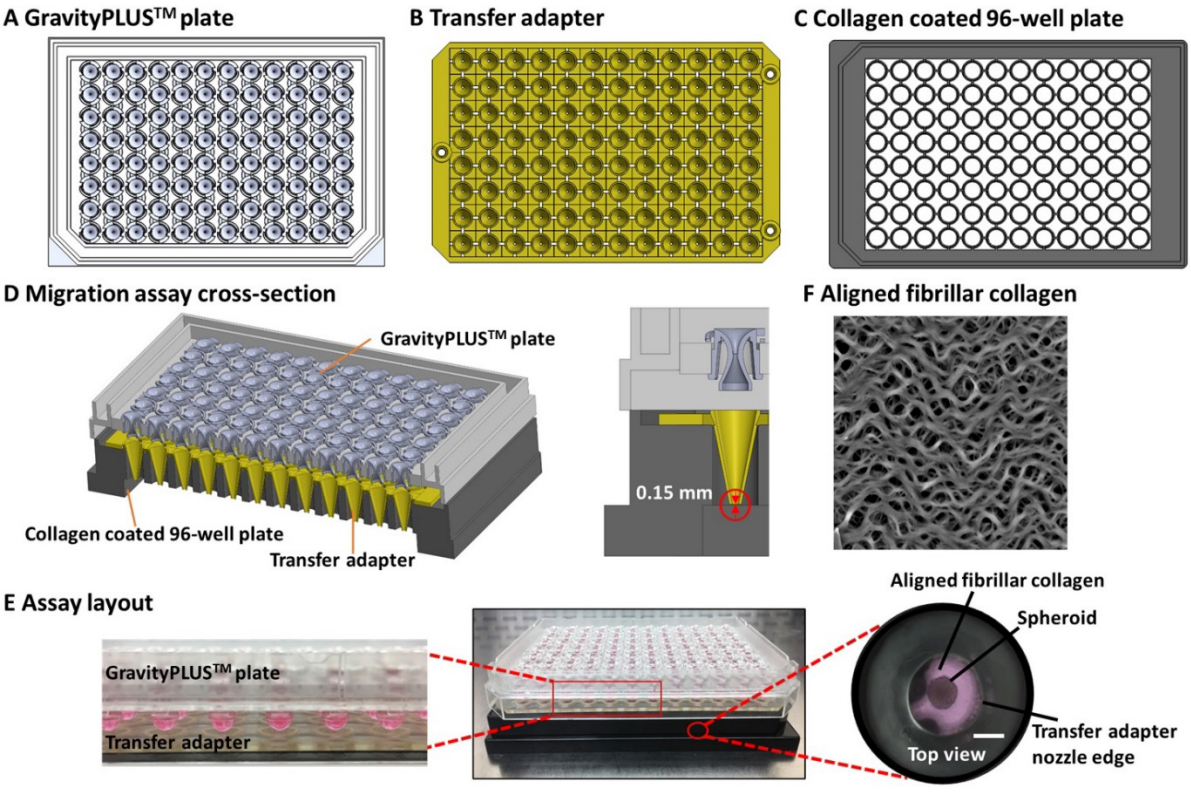

Figure 2. Spheroid assay platform integration. A: GravityPLUS™ hanging drop 96-well spheroid culture plate. B: 3D printed spheroid transfer adapter. C: Aligned fibrillar collagen

coated 96-well plate. D: 3D section view of integrated spheroid-migration assay platform. E: Assay layout (center) with hanging drops forming under the plate inlet (inset: left). Top view through the well and adapter (inset: right) with U2OS spheroid (pre-migration) positioned in the center of collagen-coated well via a 3D printed transfer adapter (right, scale bar: 400 µm). F: Representative AFM topography image (brightness adjusted height) of fibrillar collagen matrix (30 µm × 30 µm scan) as presented in Figure 1A.

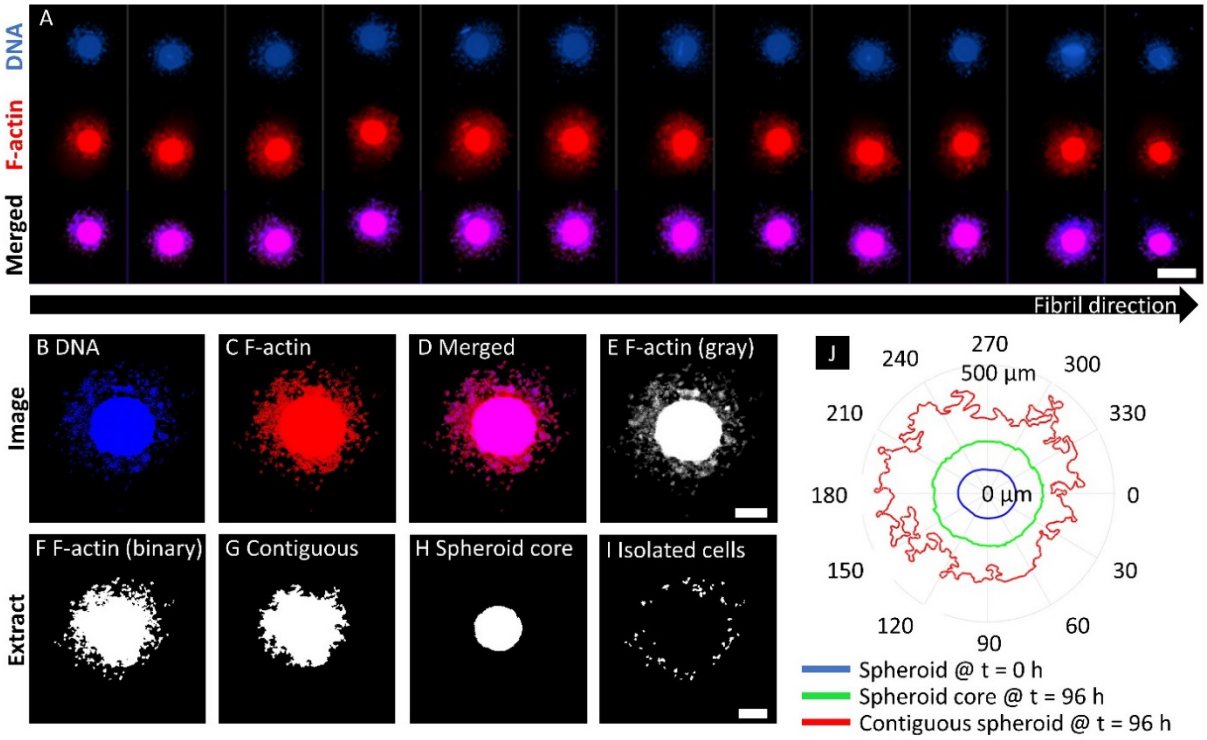

Figure 3. Spheroid outgrowth image analysis. A: High throughput imaging of the migration assay showing 12 representative spheroids at 96 h. B-D: Enlarged images of leftmost spheroid in A labelled for DNA (B), F-actin (C), and merged (D). E-I: Representative image analysis steps and output. E: Greyscale and contrast-enhanced F-actin image used for migration analysis. F: Projected spheroid cell dissemination. G: Isolated and filled contiguous spheroid outgrowth region. H: Spheroid core. I: Isolated dissociated cells. J: Polar plot depicting spheroid outgrowth at 0 h (pre-migration; blue), contiguous spheroid outgrowth at 96 h (red), and the spheroid core at 96 h (green). Scale bars: A: 1 mm, B–I: 300 µm.

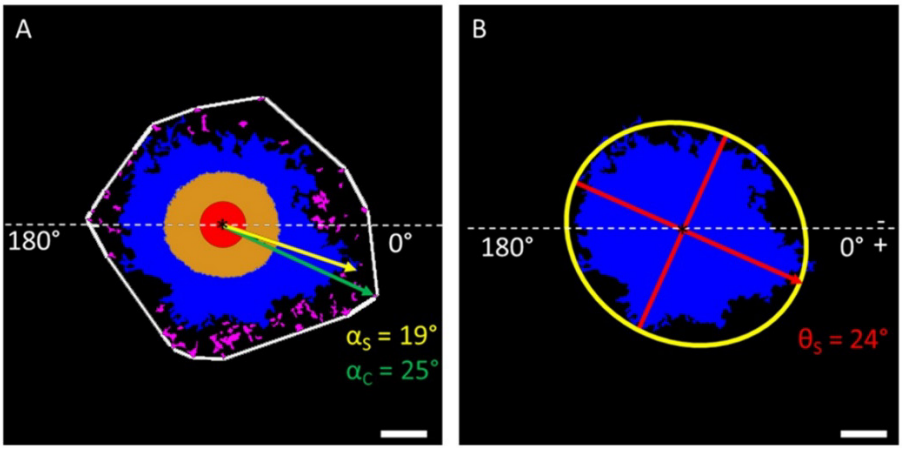

Figure 4. Representative spheroid outgrowth metrics. A: Representative spheroid dissemination depicted as projected area. The furthest extent of isolated cell migration is enclosed by a white polygon with dissociated cells indicated in magenta. Collective invasion is represented by the blue area (0.3572 mm^2). The spheroid at 0 h post transfer to ECM is represented by the red circle (105 µm equivalent radius, 0.0346 mm^2) with the asterisk denoting the centroid. The projected area of the spheroid core region at 96 h post transfer to ECM as determined by thresholding is represented by the central orange region (0.1652 mm^2). The green arrow indicates the distance to the furthest migrating cell (700 µm) and the angle, α_c, with respect to collagen orientation. The yellow line indicates the distance to the furthest point of collective protrusion (594 µm) and angle, α_S. Angles are measured clockwise from the x-axis (dashed white line), which represents collagen fibril orientation. B: Projected area of collective invasion with fitted ellipse (yellow) and major and minor axes (red), with the major axis providing the mean spheroid dissemination orientation angle, θ_s. Scale bars: 200 µm.

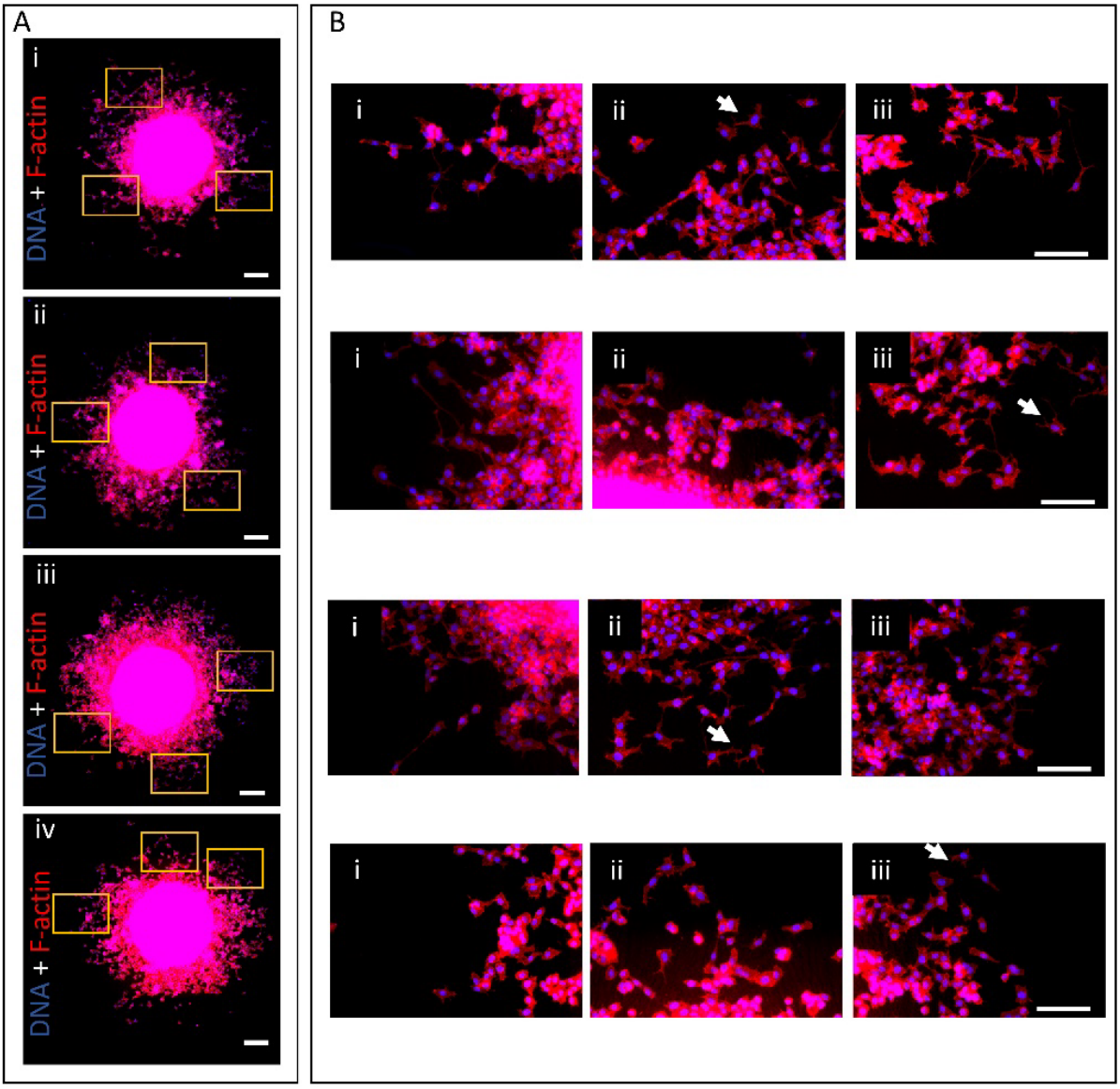

Figure 5. Single and collective cell migration from the disseminated spheroid. A: Representative images of spheroid dissemination on aligned fibrillar collagen at 96 h with heterogeneous migration modes observed including collective and single cell migration. Scale bar: 200 µm. B: (i–iii) High resolution images of regions outlined in A illustrating modes of cell migration from the spheroid mass. White arrows indicate cellular interaction with fibrillar collagen. Scale bar: 100 µm.

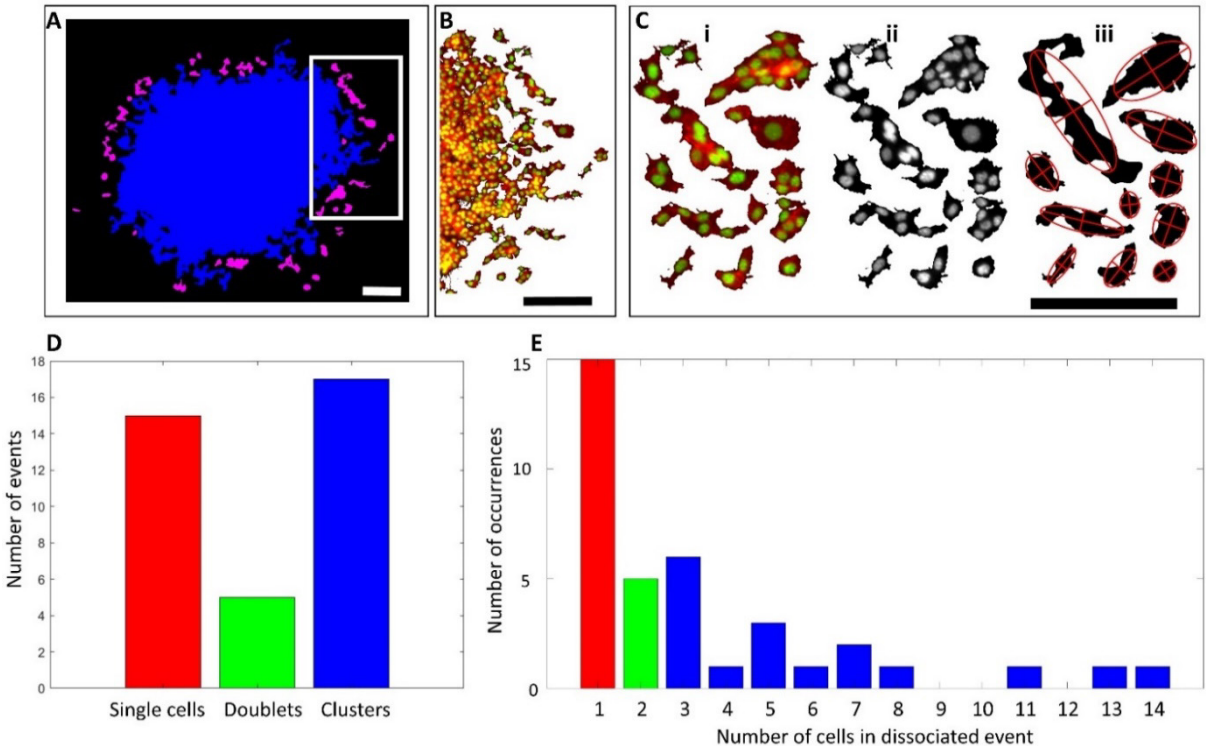

Figure 6. Analysis of migratory dissociation events in a representative spheroid. A: Segmented image with contiguous spheroid in blue and dissociated events in magenta. B: Highlighted migration from region in A with DNA (green) and F-actin (red). C: i. Extracted dissociated events from region identified in B with individual cells, doublets, and clusters evident. ii. Dissociated events converted to 8-bit greyscale image. iii. Binary image with major/minor axes and best fit ellipse overlaid. Scale bars: 200 μm. D: Distribution of number of each class of event. E: Histogram distribution of dissociation events with cell number.